Journal of Materials Chemistry A

Accepted Manuscript

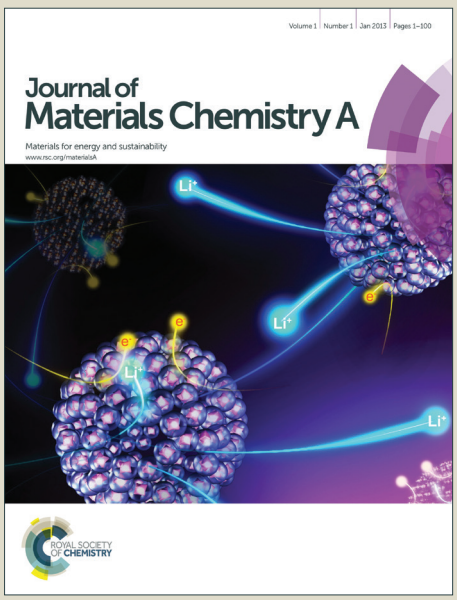

ROYAL SOCIETY OF CHEMISTRY

www.rsc.org/materialsA

Journal Name

RSCPublishing

COMMUNICATION

Sulfur-carbon yolk-shell particles based 3D interconnected nanostructure as cathode material for rechargeable lithium-sulfur batteries

Cite this: DOI: 10.1039/x0xx00000x

Received 00th January 2012,
Accepted 00th January 2012

DOI: 10.1039/x0xx00000x

www.rsc.org/

Ning Ding,[‡a] Yanwei Lum,[‡a] Shaofeng Chen,[b] Sheau Wei Chien,[a] T. S. Andy Hor,[ac] Zhaolin Liu,[*a] and Yun Zong[*a]

The preparation of cathode materials for rechargeable lithium-sulfur batteries generally involves melt-diffusion or vapor-phase infusion of sulfur into the pores of nanostructured carbon. There are clear drawbacks of these two approaches. Firstly, the control over the filling content of sulfur into the voids is poor, which noticeably compromises the battery capacity; Secondly, a significant portion of sulfur unavoidably lands on the outer surface of carbon as unprotected sulfur that contributes readily to the redox shuttle, resulting in fast decay of the battery capacity. Herein, we report for the 1st time a novel method to synthesize sulfur-carbon yolk-shell particles with sulfur fully confined inside the conductive carbon shells, and the filling content of sulfur can be well-controlled and fine-tuned. In the yolk-shell structure the sulfur spheres partially occupy the internal void space of highly conductive carbon, allowing for comfortable accommodation of the volume expansion of sulfur upon lithiation during the battery discharge process. 3D interconnected nanostructure based on such sulfur-carbon yolk-shell particles exhibits a high initial capacity of 560 mAh g^{-1} (per gram electrode) with good cycling performance, promising high potential in rechargeable lithium-sulfur batteries for a wide range of applications.

Introduction

Lithium-sulfur (Li-S) batteries are considered to be the most viable option for the next-generation high-energy rechargeable batteries. Li-S batteries can deliver a practical energy density of 400-600 Wh kg^{-1} which is 2~3 times as high as that of commercially available Li-ion batteries;[1-6] however, the commercialization of Li-S batteries is hindered by the fast decay of the battery capacity which is caused by the precipitation of the dissolved discharge products (polysulfides) onto the lithium anode.[7] This issue is mitigable if an effective conductive host can be introduced to confine sulfur and polysulfides during the charge and discharge processes, respectively. For the host, nanostructured carbon matrix with pores is a popular choice due to its high surface area and good electric conductivity. Conventionally, sulfur is introduced into the pores within the carbon matrix via melt-diffusion or vapor-phase infusion, and the obtained sulfur/carbon (S/C) composites exhibit improvement in the cycling performance.[8-21] Nevertheless, such melting diffusion and infusion processes bring in three clear drawbacks: (i) some sulfur will inevitably land on the outer surface of the host material as unprotected sulfur that contributes to the redox shuttle, resulting in a large capacity loss for the first several cycles;[22] (ii) pores with little or no sulfur inside hardly contribute to the battery capacity, comprising the specific capacity per gram of electrode accordingly; (iii) pores with sulfur filling greater than 60% of void will not be able to accommodate the volume expansion of sulfur upon lithiation ($S \rightarrow Li_2S$, ~80% of volume increase), resulting in fracture in the carbon host and leakage of polysulfides. Moreover, the isolated Li_2S particles formed in the discharge process will not participate in the subsequent charge process, appearing as decay in the battery capacity.[23] Thus, approaches that lead to sulfur confinement with a well-defined structure, including controlled void volume within the confined

space around sulfur particles, and low portion of mispositioned sulfur particles are highly in demand.

The first realization of such novel structure was demonstrated by Cui et al via sulfur@TiO_2 yolk-shell nanoparticles which were proven as a superior cathode for Li-S batteries with excellent cycling stability.[24] The group also developed an alternative approach to confine sulfur with void in the form of hollow sulfur nanoparticles coated with a thin layer of polyvinylpyrrolidone that gave similar promise.[25] The sulfur-based yolk-shell nanostructure was further developed using a conducting polymer shell, polyaniline, and the cycling stability was demonstrated in Li-S batteries.[26] For high rate operation of large rechargeable Li-S batteries, a highly conductive coating of carbon (4 S cm^{-1})[27] that is also electrochemically stable and low cost appears as a natural choice. The unavailability of conductive carbon coated nanosized sulfur to date, however, is mainly due to the fact that the minimum temperature (600 °C) required to form a conductive carbon shell via carbonization of a carbohydrate precursor is much higher than the boiling point of sulfur (444.6 °C), such that sulfur will vigorously evaporate and quickly vanish before the carbonization temperature is reached. In fact, any coating on sulfur particles that needs to form at temperature above the melting point of sulfur (115.2 °C) would impose issues, as the original size and morphology of the sulfur particles will be completely lost in this case. Exceptions are the hydro-/solvo-thermal processes, through which low temperature carbonization is possible (120-250 °C) and hydrocarbons with low electronic conductivity are generally produced.[28,29] Herein, we report for the 1st time a novel method to synthesize sulfur-carbon yolk-shell particles with sulfur fully confined in the conductive carbon shells, and the filling content of sulfur can be well-controlled and fine-tuned. In the yolk-shell structure the sulfur spheres partially occupy the void inside the carbon shell, allowing for comfortable accommodation of the volume expansion of sulfur upon lithiation during the battery discharge process.[30] The 3D interconnected nanostructure based on such sulfur-carbon yolk-shell particles exhibits a high initial capacity with good cycling performance in rechargeable lithium-sulfur batteries.

Results and discussion

The S@C yolk-shell particles and such particles based 3D interconnected nanostructure were synthesized through an indirect pathway, as schematically shown in Figure 1 (a→d). In general, uniform and thermally stable metal sulfide (MS) spheres of a few hundreds nm in diameter were prepared via a hydrothermal reaction, and taken as the sulfur precursor and the template particles. Acetone solution of phenol formaldehyde (PF) resin was used to disperse these particles and form a uniform suspension. As drying at ambient condition, the MS particles self-assemble, with PF resin filling the inter-particle interstices homogeneously. The dried PF resin was converted into highly conductive carbon coatings via a carbonization process to produce MS@C. By soaking MS@C in the aqueous solution of a mild oxidant, e.g. $Fe(NO_3)_3$, MS is oxidized to form sulfur particles inside the carbon shells with departure of free M^{2+} (Equation 1) through the micropores on the carbon shells, leaving voids inside which are able to comfortably accommodate the volume expansion of sulfur upon lithiation in the discharge process of Li-S batteries (Figure 1, d→e).

$$MS_{(s)} + 2Fe^{3+}_{(aq)} \rightarrow M^{2+}_{(aq)} + S_{(s)} + 2Fe^{2+}_{(aq)} \qquad (1)$$

The choice of metal sulfide is based on the following criterion: (i) high melting point and high decomposition temperature in a reducing atmosphere, in order to ensure smooth formation of carbon shell during the carbonization process; (ii) small solubility product constant (K_{sp}) such that the MS particles can be obtained in high yield; (iii) environmental benignity which is required for large scale industry production; (iv) low cost and earth abundance to allow for price competitiveness and economically viable. Zinc sulfide (ZnS) stands out from a wide range of metal sulfides (cf. Tab. S1), and was adopted in the synthesis of the S@C yolk-shell nanostructures.

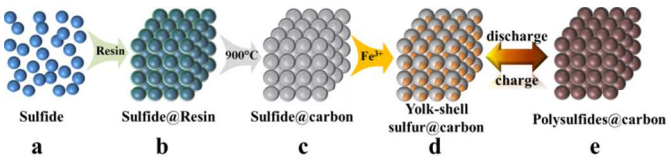

Figure 1 Schematic illustration on the synthesis of S@C yolk-shell nanostructures (a→d) and the volumetric expansion of sulfur upon lithiation (d→e) during the discharge processes of rechargeable Li-S batteries.

The ZnS spheres were produced by reacting zinc acetate and thiourea under hydrothermal condition, and found typically ~300 nm in diameter (Figure S1a). TEM images (Figure S1b) revealed these uniform ZnS particles as secondary particles of the self-assembled primary ZnS nanoparticles with a diameter of 4~5 nm. The ZnS spheres were dispersed into an acetone solution containing PF resin,

and the suspension was slowly dried at room temperature whereby the ZnS particles self-assembled with PF resin filled their interstices. The obtained ZnS@PF resin composite was then carbonized in an argon atmosphere at 900 °C for 1 h, whereby 3D interconnected carbon-coated ZnS spheres (ZnS@C) formed (Figure S1c). During carbonization process, the primary ZnS nanoparticles inclined to grow into larger particles and a large portion of grain boundary disappeared leaving more void space. As a consequence, the ZnS spheres (secondary particles) exhibit a "hollow-like" structure (Figure S1d) that facilitates the conversion of ZnS into sulfur and Zn^{2+}.

The sulfide→S conversion reaction was conducted by soaking ZnS@C composite in aqueous solution of ferric nitrate, in which the chemical reaction shown in Equation 2 takes place.[31] The sulfur particles formed are confined inside the carbon shell, with free zinc ions leeching out into the solution that is eventually washed away using deionized water in the post purification process.

$$2Fe^{3+}_{(aq)} + ZnS_{(s)} \rightarrow 2Fe^{2+}_{(aq)} + Zn^{2+}_{(aq)} + S_{(s)} \qquad (2)$$

Based on formula the loss of zinc ions essentially removes ~2/3 of the total mass of ZnS spheres. The produced element sulfur with a much lower material density (compared to that of ZnS), however, will compensate some of the volume loss inside the carbon shells. Theoretically, a full conversion of carbon coated single crystal ZnS spheres will lead to a volume reduction of 34.7%. As ZnS spheres in this work are indeed secondary particles with a "hollow-like" structure, comprising large number of primary ZnS nanoparticles with inter-nanoparticle interstices, the formation of voids with larger volume reduction in the experiment is anticipated. The size of such voids inside the carbon shells can be further enlarged via the control over the extent of sulfide→S conversion which is further dictated by the factors such as the concentration of ferric nitrate, the soaking time, etc. The unreacted ZnS residue inside the carbon shells can be easily removed by soaking the particles in diluted aqueous solution of an acid, e.g. HCl.

The process of ZnS to sulfur conversion inside the carbon shells was investigated using TEM. Using $Fe(NO_3)_3$ solution of 5 different concentrations, ZnS-S@C nanostructures with different extent of ZnS→S conversion were obtained and their TEM images are shown in Figure 2a-f. One can see that the conversion process started off uniformly on the ZnS spheres (Figure 2b), followed by a continuous shrinkage (Figure 2c-e), and eventually evolved to a sulfur sphere with a diameter of 150 nm which resides on the inside wall of the carbon shell as a "yolk". The spacious void around the yolk is sufficiently large to accommodate the volume expansion of sulfur upon lithiation (volume increase by ~80%). Due to the low electron contrast of sulfur to carbon in the TEM images, it was difficult to specify the exact locations of sulfur in the oxidized intermediates until the conversion was complete (Figure 2f).

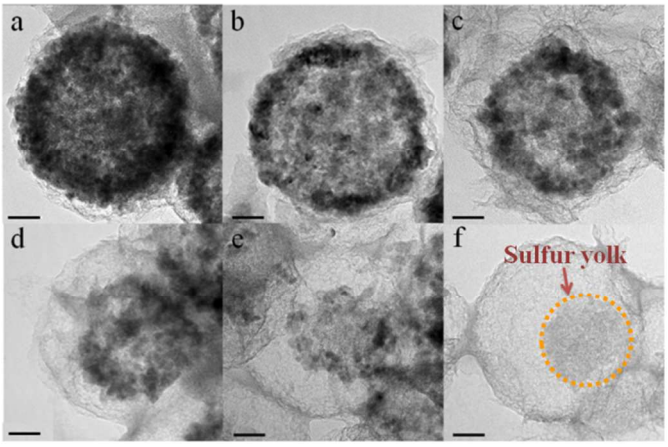

Figure 2 TEM images of the carbon encapsulated ZnS sphere at different stages of the ZnS→S conversion. (a) Carbon encapsulated ZnS sphere with a "hollow-like" structure. (b) The ZnS sphere starts to thin out after soaking in 0.4 M $Fe(NO_3)_3$. (c) The thinned ZnS sphere starts to shrink noticeably and further thins out after soaking in 0.8 M $Fe(NO_3)_3$. (d) More thinning and shrinkage were observed, after the thinned and shrunk ZnS spheres were soaked in 1.2 M $Fe(NO_3)_3$. (e) The thinned and shrunk ZnS collapsed after soaking in 1.6 M $Fe(NO_3)_3$. (f) The product of full conversion, S@C yolk-shell nanostructure formed after soaking in 2.0 M $Fe(NO_3)_3$. All the scale bars are 50 nm.

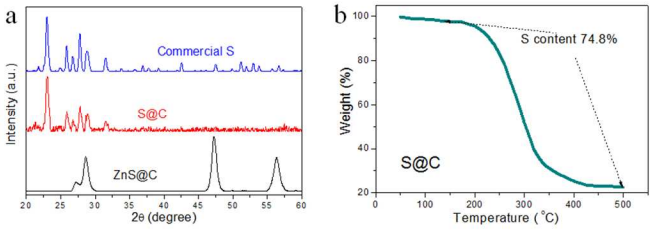

Figure 3 (a) XRD patterns of ZnS@C, the final oxidation product S@C, and the commercial orthorhombic phase crystalline sulfur (reference). The key patterns of S in S@C match well with that of the commercial sulfur. (b) TGA curve of a representative S@C yolk-shell composite with a sulfur load of 74.8%. The TGA experiment was conducted under nitrogen atmosphere.

The structure of ZnS@C and S@C composites was characterized and confirmed by powder XRD patterns (Fig. 3a). The ZnS particles

exhibit a cubic phase (zinc blende) with 3 strong peaks located at 28.5°, 47.2° and 56.4°, which correspond to the crystal planes of (111), (220) and (311), respectively. The size of primary particles of ZnS in ZnS@C was calculated to be ~11 nm according to the Scherrer's equation. The increased size of ZnS primary nanoparticles (compared to the ones obtained directly from hydrothermal reaction) mainly arises from the sintering-type of growth at high temperature when PF resin was carbonized at 900 °C. Nevertheless, these ZnS nanoparticles are small enough to be reactive, which facilitates fast conversion of sulfide to sulfur. For S@C, the diffraction peaks match well with the XRD pattern of commercial orthorhombic phase crystalline sulfur, proving successful conversion of sulfide to sulfur. The elemental mapping confirms the formation of S@C yolk-shell nanostructures (Fig. S2). Thermogravimetric analysis (TGA) result suggests that the sulfur content can be as high as 74.8 wt% in the S@C composite (Fig. 3b), which is reflected as the mass loss between 150 and 500 °C whereby the sulfur evaporated gradually.

The carbon content in the S@C yolk-shell nanostructures can be tuned by varying the amount of PF resin while keeping the mass of ZnS spheres constant. In the experiment, PF resin solution of 0.1, 0.2, 0.4 and 0.5 ml were introduced to 0.5 gram of ZnS spheres, respectively. Similar processes were followed to produce S@C yolk-shell nanostructures of different carbon content which are denoted as SC1, SC2, SC3 and SC4 (from low to high carbon content), respectively. The actual carbon contents in these S@C yolk-shell nanostructures were determined by TGA analyses (Tab. S2) and found tuneable between 25.2 to 66.2 wt%, which demonstrates the powerful feature of our approach. From SC1 to SC4, the increase of carbon content leads to thicker carbon shells (Figure 4) which more effectively mitigate the leakage of polysulfides during the discharge process thus improved cycling stability; however, the decreased sulfur loading results in lower battery capacity. As S/C composite with low carbon content and high sulfur content is desirable for high specific capacity in batteries while polysulfide leakage mitigation through thick carbon shell helps the cycling performance of batteries, it is crucial to balance the sulfur content and the carbon shell thickness to enable the formation of a continuous carbon matrix with maximized sulfur content. This can be achieved by precisely controlling the mass ratio of PF resin to ZnS spheres in the initial synthesis as extensively discussed above.

The cycling performance of the S@C yolk-shell nanostructures in Li-S batteries was investigated and the results are shown in Figure 5a. The initial discharge capacity of SC1, SC2, SC3 and SC4 were found to be 878, 796, 548, and 443 mAh per gram of electrode (including S@C composite, carbon black and binder), respectively. All the four samples show the coulombic efficiency close to 100% and the galvanostatic discharge-charge curves for the first three cycles are shown in Figure S3. It is worth noting that the capacity of SC1 and SC2 is higher than previously reported results in literatures (typically about 500 mAh g^{-1}, based on the total mass of all components on cathode).[10,24,25,32] The higher capacity is partially introduced by the addition of Li_2S_6, which was used as electrolyte

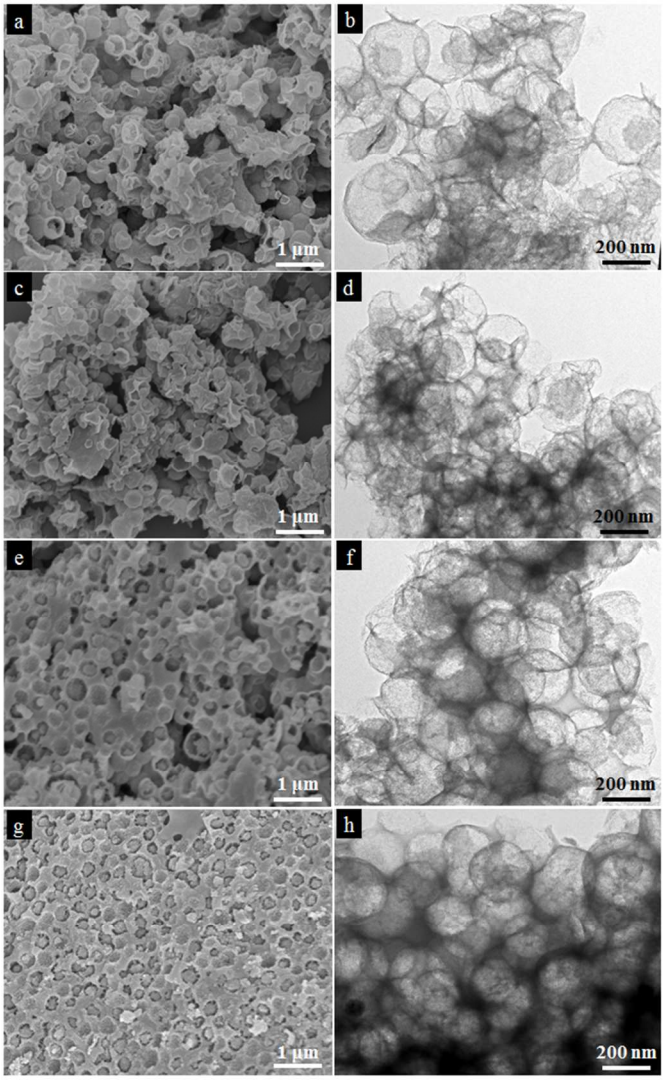

Figure 4 Representative SEM (a, c, e, g) and TEM (b, d, f, h) images of the S@C yolk-shell nanostructured material prepared using different amount of phenol formaldehyde resin and thus possess different carbon content. (a, b) SC1, carbon content: 25.2 wt%. (c, d) SC2, carbon content: 46.0 wt%. (e, f) SC3, carbon content: 57.1 wt%. (g, h) SC4, carbon content: 66.2 wt%. The carbon shells are generally thicker for higher carbon content.

additive to enhance the battery cyclability[33,34] and may precipitate on carbon black and the carbon shell as sulfur during charging process. To calibrate the areal battery capacity, samples with only carbon shell prepared by directly removing ZnS from ZnS@C (the precursor of SC1) via acid treatment was used as electrode materials, and the battery cycling performance is shown in Figure S4. One can see that the capacity resulted from Li_2S_6 is at most 320 mAh g^{-1}. Taking this as a reference, the maximum capacity of sulfur-carbon yolk-shell is obtained as ~560 mAh per gram of electrode or 1400 mAh per gram of sulfur in S@C yolk-shell nanostructure which is reasonably high.

Similar slow capacity decay is seen for SC2 to SC4 with thicker carbon shells, while a faster decay of capacity is visible for SC1 that possesses the thinnest carbon shell. The less desirable cycling stability of SC1 is anticipated, as the thin carbon shell may be inadequate to prevent polysulfides from leaking out of the carbon spheres. This proves the importance of a balanced sulfur and carbon content to equip Li-S batteries with high capacity and satisfactory cyclability, and the optimal S/C ratio in this study was found to be ~ 1:1. In a control experiment, hollow carbon spheres were prepared by soaking S@C yolk-shell (SC2) in toluene, whereby the sulfur yolks inside the carbon shells are completely removed. Elemental sulfur was then introduced to the hollow carbon spheres via melt-diffusion method to form a control sample, denoted as Melting-diffused Sulfur in Carbon (MSC). Unsurprisingly, MSC exhibits poor uniformity in its morphology, as shown in a representative SEM image (Fig. 5b) in which micron-sized sulfur particles are seen sitting on the surface of carbon matrix. With sulfur being an insulator, such micron-sized particles give poor electrical contact in the electrode which lowers the utilization rate of the available sulfur, leading to a much lower battery capacity. This is clearly seen in Fig. 5a, in which MSC with 50.0 wt% load of sulfur displays a capacity lower than that of SC4 with sulfur load of 33.8 wt%. The faster decay in the capacity (in comparison to CS4) is likely attributed to the unprotected sulfur on the carbon shell surface that contributes to the redox shuttles. Hence, it is rather clear that the 3D interconnected carbon-encapsulated sulfur based on S@C yolk-shell nanostructure, prepared via an indirect ZnS precursor approach, is a superior choice of sulfur cathode.

Conclusion

In summary, we have developed an indirect method to prepare S@C yolk-shell particles and 3D interconnected nanostructure based on such particles. The voids around the yolks inside the carbon shells are able to comfortably accommodate the expansion of sulfur upon lithiation during battery discharge process, and the carbon coating can effectively prevent the polysulfide from leaking out into the electrolyte. Cathodes of such S@C yolk-shell materials exhibit high initial capacities and good cycling performance. As a clear contrast to the conventional melt-diffusion method, our approach not only provides much better confinement for the sulfur particles inside the pores, but also prevents bulk sulfur particles formation on the surfaces of carbon matrix. Both features are crucial to good cycling performance of Li-S batteries. This new method will shed a light on the synthesis of other carbon-coated novel nanostructures for future high performance Li-S batteries.

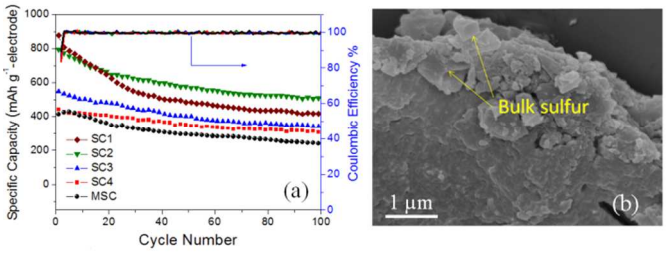

Figure 5 (a) Performance data of Li-S batteries using electrode of S@C yolk-shell composites with different carbon content (SC1 to SC4) and the control sample prepared via melting-diffusion of sulfur (MSC). Faster capacity decay is seen for S@C with thinnest carbon shell (SC1, lowest carbon content). Control sample (MSC) gives the lowest capacity. (b) SEM image of MSC, where the bulk sulfur particles landed on the surface of the porous carbon are marked.

Acknowledgements

This work is supported by the Advanced Energy Storage Research Programme (IMRE/12-2P0503 and IMRE/12-2P0504), Institute of Materials Research and Engineering (IMRE) of the Agency for Science, Technology and Research (A*STAR), Singapore. We express sincere thanks to Ms. Huiru Tan for elemental mapping.

Notes and references

[a]*Institute of Materials Research and Engineering (IMRE), A*STAR (Agency for Science, Technology and Research), 3 Research Link, Singapore 117602, Republic of Singapore. E-mail: y-zong@imre.a-star.edu.sg; zl-liu@imre.a-star.edu.sg*

[b]*Division of Nanomaterials and Chemistry, Hefei National Laboratory for Physical Sciences at Microscale, University of Science and Technology of China, Hefei 230026, P.R. China.*

[c]*Department of Chemistry, National University of Singapore, 3 Science Drive 3, Singapore 117543, Republic of Singapore*.

[‡]*These authors contributed equally to this work.*

† Electronic Supplementary Information (ESI) available: Experimental section to synthesize S@C yolk-shell nanostructures, additional SEM and TEM images of ZnS and ZnS@C, elemental mapping of sulfur and carbon, capacity calibration and results of thermal gravimetric analyses. See DOI: 10.1039/c000000x/

1 P. G. Bruce, S. A. Freunberger, L. J. Hardwick and J. M. Tarascon, *Nat. Mater.,* 2012, **11,** 19-29.
2 X. Ji and L. F. Nazar, *J. Mater. Chem.,* 2010, **20,** 9821-9826.
3 S. Evers and L. F. Nazar, *Acc. Chem. Res.,* 2013, **46,** 1135-1143.
4 A. Manthiram, Y. Fu and Y. S. Su, *Acc. Chem. Res.,* 2013, **46,** 1125-1134.
5 Y. Yang, G. Zheng and Y. Cui, *Chem. Soc. Rev.,* 2013, **42,** 3018-3032.
6 Y. X. Yin, S. Xin, Y. G. Guo and L. J. Wan, *Angew. Chem. Int. Ed.,* 2013, **52,** 13186-13200.
7 Y. V. Mikhaylik, J. R. Akridge, *J. Electrochem. Soc.,* 2004, **151,** A1969-A1976.
8 G. He, X. Ji and L. F. Nazar, *Energy Environ. Sci.,* 2011, **4,** 2878-2883.
9 N. Jayaprakash, J. Shen, S. S. Moganty, A. Corona and L. A. Archer, *Angew. Chem. Int. Ed.*, 2011, **50,** 5904-5908.
10 L. Ji, M. Rao, H. Zheng, L. Zhang, Y. Li, W. Duan, J. Guo, E. J. Cairns and Y. Zhang, *J. Am. Chem. Soc.,* 2011, **133,** 18522-18525.
11 J. T. Lee, Y. Zhao, S. Thieme, H. Kim, M. Oschatz, L. Borchardt, A. Magasinski, W. Cho, S. Kaskel and G. Yushin, *Adv. Mater*., 2013, **25,** 4573-4579.
12 G. C. Li, G. R. Li, S. H. Ye and X. P. Gao, *Adv. Energy Mater.,* 2012, **2,** 1238-1245.
13 C. Liang, N. J. Dudney and J. Y. Howe, *Chem. Mater.,* 2009, **21,** 4724-4730.
14 S. Xin, L. Gu, N. H. Zhao, Y. X. Yin, L. J. Zhou, Y. G. Guo and L. J. Wan, *J. Am. Chem. Soc.,* 2012, **134,** 18510-18513.
15 B. Zhang, X. Qin, G. Li and X. Gao, *Energy Environ. Sci.,* 2010, **3,** 1531-1537.
16 G. Zheng, Y. Yang, J. J. Cha, S. S. Hong and Y. Cui, *Nano Lett.,* 2011, **11,** 4462-4467.
17 G. Zhou, S. Pei, L. Li, D. W. Wang, S. Wang, K. Huang, L. C. Yin, F. Li and H. M. Cheng, *Adv. Mater.,* 2014, **26,** 625-631.
18 R. Elazari, G. Salitra, A. Garsuch, A. Panchenko, D. Aurbach, *Adv. Mater.,* 2011, **23,** 5641-5644.
19 Y. Yang, G. Yu, J. J. Cha, H. Wu, M. Vosgueritchian, Y. Yao, Z. Bao and Y. Cui, *ACS Nano,* 2011, **5,** 9187-9193.
20 H. Yao, G. Zheng, W. Li, M. T. McDowell, Z. She, N. Liu, Z. Lu and Y. Cui, *Nano Lett.,* 2013, **13,** 3385-3390.
21 J. Schuster, G. He, B. Mandlmeier, T. Yim, K. T. Lee, T. Bein and L. F. Nazar, *Angew. Chem. Int. Ed.,* 2012, **51,** 3591-3595.
22 M. Hagen, S. Dorfler, H. Althues, J. Tubke, M. J. Hoffmann, S. Kaskel and K. Pinkwart, *J. Power Sources,* 2012, **213,** 239-248.
23 S. E. Cheon, K. S. Ko, J. H. Cho, S. W. Kim, E. Y. Chin and H. T. Kim, *J. Electrochem. Soc.,* 2003, 150, A800-A805.
24 Z. W. Seh, W. Li, J. J. Cha, G. Zheng, Y. Yang, M. T. McDowell, P. C. Hsu and Y. Cui, *Nat. Commun.,* 2013, **4,** 1331.
25 W. Li, G. Zheng, Y. Yang, Z. W. She, N. Liu and Y. Cui, *Proc. Natl. Acad. Sci. U. S. A.,* 2013, **110,** 7148-7153.
26 W. Zhou, Y. Yu, H. Chen, F. J. DiSalvo and H. D. Abruna, *J. Am. Chem. Soc*., 2013, **135,** 16736-16743.
27 H. Byun, G. Nam, Y. M. Rhym and S. E. Shim, *Carbon Lett*., 2012, **13,** 94-98.
28 Q. Wang, H. Li, L. Q. Chen and X. J. Huang, *Carbon,* 2001, **39,** 2211-2214.
29 M. Sevilla and A. Fuertes, *Carbon,* 2009, **47,** 2281-2289.
30 N. Ding, Y.W. Lum, T.S.A. Hor, Z. L. Liu and Y. Zong, SG Patent 10201402315P.
31 P. C. Rath, R. K. Paramguru, P. K. Jena, *Hydrometallurgy,* 1981, **6,** 219-225.
32 W. J. Chung, J. J. Griebel, E. T. Kim, H. Yoon, A. G. Simmonds, H. J. Ji, P. T. Dirlam, R. S. Glass, J. J. Wie, N. A. Nguyen, B. W. Guralnick, J. Park, A. Somogyi, P. Theato, M. E. Mackay, Y. E. Sung, K. Char, J. Pyun, *Nat. Chem.,* 2013, **5,** 518-524.
33 R. Xu, I. Belharouak, J. C. M. Li, X. Zhang, I. Bloom, J. Bareno, *Adv. Energy Mater.,* 2013, **3,** 833-838.
34 X. B. Cheng, J. Q. Huang, H. J. Peng, J. Q. Nie, X. Y. Liu, Q. Zhang, F. Wei, *J. Power Sources,* 2014, **253,** 263-268.

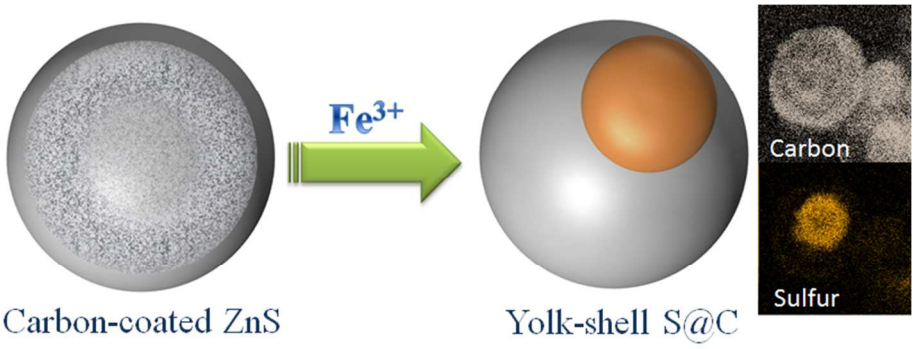

A novel 3D interconnected sulfur-carbon yolk-shell nanostructure synthesized via mild oxidation of carbon-coated zinc sulfide is able to accommodate the volume expansion of sulfur upon lithiation during the discharge of Li-S battery, giving high capacity with excellent cycling performance.